ARTICLE
PUBLISHED ONLINE: 19 MAY 2013 | DOI: 10.1038/NCHEMBIO.1257

nature chemical biology

Inhibitors that stabilize a closed RAF kinase domain conformation induce dimerization

Hugo Lavoie[1,8], Neroshan Thevakumaran[2,3,8], Gwenaëlle Gavory[1], John J Li[2,4], Abbas Padeganeh[1], Sébastien Guiral[1], Jean Duchaine[1], Daniel Y L Mao[2,5], Michel Bouvier[1,6], Frank Sicheri[2–4]* & Marc Therrien[1,7]*

RAF kinases have a prominent role in cancer. Their mode of activation is complex but critically requires dimerization of their kinase domains. Unexpectedly, several ATP-competitive RAF inhibitors were recently found to promote dimerization and transactivation of RAF kinases in a RAS-dependent manner and, as a result, undesirably stimulate RAS/ERK pathway–mediated cell growth. The mechanism by which these inhibitors induce RAF kinase domain dimerization remains unclear. Here we describe bioluminescence resonance energy transfer–based biosensors for the extended RAF family that enable the detection of RAF dimerization in living cells. Notably, we demonstrate the utility of these tools for profiling kinase inhibitors that selectively modulate RAF dimerization and for probing structural determinants of RAF dimerization *in vivo*. Our findings, which seem generalizable to other kinase families allosterically regulated by kinase domain dimerization, suggest a model whereby ATP-competitive inhibitors mediate RAF dimerization by stabilizing a rigid closed conformation of the kinase domain.

Dysregulation of the RAS-RAF-MEK-ERK pathway is conducive to tumor formation[1,2]. Although activating mutations in the *RAS* genes (*HRAS*, *KRAS* and *NRAS*) are the most recurrent lesions driving oncogenic RAS/ERK signaling, gain-of-function mutations in *BRAF* are arguably among the leading causes[3,4]. Under normal conditions, RAF activation is initiated at the plasma membrane by binding growth factor–stimulated RAS GTPases. This triggers the sequential phosphorylation and activation of MEK and ERK. Active ERK then phosphorylates a diverse set of substrates, eliciting various cell-specific responses including proliferation and survival.

Mammals express three RAF paralogs (ARAF, BRAF and CRAF) and two closely related proteins (KSR1 and KSR2), herein referred to as RAF family members[5]. A recently discovered feature of RAS-mediated RAF activation involves the homo- or heterodimerization of the kinase domain of RAF family members through a conserved side-to-side interface[6–9]. The mechanism by which dimerization induces catalytic activity has not been elucidated, but it most likely involves allosteric switching of the respective protomers[7].

Given its involvement in tumorigenesis, several inhibitors of RAF have been developed[10]. Selective inhibitors of $BRAF^{V600E}$ (a frequent BRAF oncogenic variant) are now available, and clinical activity against $BRAF^{V600E}$-dependent metastatic melanomas has been observed with one of them called vemurafenib (PLX4032)[11,12]. Regrettably, two shortcomings have emerged. First, virtually all of the inhibitors tested to date promote RAS-dependent RAF dimerization and, in a dose-dependent manner, increase ERK signaling and cell growth[13–15]. Apparently, drug-bound RAF protomers dimerize with and transactivate drug-free protomers, leading to enhanced signaling[16]. This situation warns against using current RAF inhibitors to treat RAS-dependent cancers. Second, resistance to vemurafenib invariably develops within a year, and one frequent mechanism driving resistance involves RAF dimerization[17,18]. Clearly, RAF dimerization is a critical parameter to consider when designing compounds targeting RAS/ERK–dependent tumors.

Current methods for monitoring RAF dimerization are based on low-throughput assays[6–9] that are ill adapted for surveying numerous samples or conditions or for screening large libraries. Here, we developed bioluminescence resonance energy transfer (BRET)-based biosensors enabling quantitative detection of kinase domain dimerization of each RAF family member in living cells. The system recapitulates known genetic and pharmacological perturbations of RAF dimerization with high specificity, sensitivity and robustness. Pairwise assays revealed discrete dimerization capabilities for each RAF family member. In drug profiling experiments, the biosensors provided a snapshot of the complex and varied effects that inhibitors have on the RAF dimerization network and therefore informed on the potential *in vivo* consequences of an inhibitor. In a high-throughput setting, these biosensors unveiled unforeseen off-target effects of diverse ATP-competitive kinase inhibitors on RAF dimerization. On the basis of biophysical characterization of a subset of these inhibitors and crystallographic data, we propose that ATP-competitive RAF inhibitors directly promote dimerization by stabilizing a closed conformation of the kinase domain.

RESULTS

Engineering RAF dimerization biosensors

RAF dimerization biosensors were developed using the BRET2 system, which allows real-time monitoring of protein-protein interactions in living cells[19]. Isolated RAF kinase domains have the propensity to form dimers in solution in a RAS-independent manner[7]. We thus used the CRAF kinase domain ($CRAF_{KD}$) as a starting point, which we fused to the N or C terminus of *Renilla* luciferase variant II (RlucII; donor moiety) or GFP10 (acceptor moiety)[20,21].

[1]Institute for Research in Immunology and Cancer, Laboratory of Intracellular Signalling, Université de Montréal, Montréal, Québec, Canada. [2]Samuel Lunenfeld Research Institute, Mount Sinai Hospital, Toronto, Ontario, Canada. [3]Department of Biochemistry, University of Toronto, Toronto, Ontario, Canada. [4]Department of Molecular Genetics, University of Toronto, Toronto, Ontario, Canada. [5]Department of Chemistry and Biology, Ryerson University, Toronto, Ontario, Canada. [6]Département de biochimie, Université de Montréal, Montréal, Québec, Canada. [7]Département de pathologie et biologie cellulaire, Université de Montréal, Montréal, Québec, Canada. [8]These authors contributed equally to this work. *e-mail: sicheri@lunenfeld.ca or marc.therrien@umontreal.ca

These constructs produced relatively weak BRET signals when tested by transient transfections in HEK293T cells (not shown). To improve signal output, we added a membrane-targeting CAAX box to the C terminus of the fusion proteins to increase the effective concentration of the interacting pairs in a bidimensional space. CAAX box–containing $CRAF_{KD}$ constructs with N-terminal donor and acceptor fusions led to higher BRET signals that were saturable in titration experiments, unlike noninteracting probes, which served as a reference for nonspecific interactions (**Fig. 1a**). Membrane-targeted $BRAF_{KD}$ constructs also produced saturable BRET signals (**Fig. 1b**,**c**; for simplicity, the term CAAX is omitted in the construct names described hereafter) that clearly depended on membrane targeting (**Supplementary Results**, **Supplementary Fig. 1a**,**b**) and did not fluctuate linearly in response to the total amount of the interacting probes (**Supplementary Fig. 1c**), as generally observed for nonspecific interactors[22].

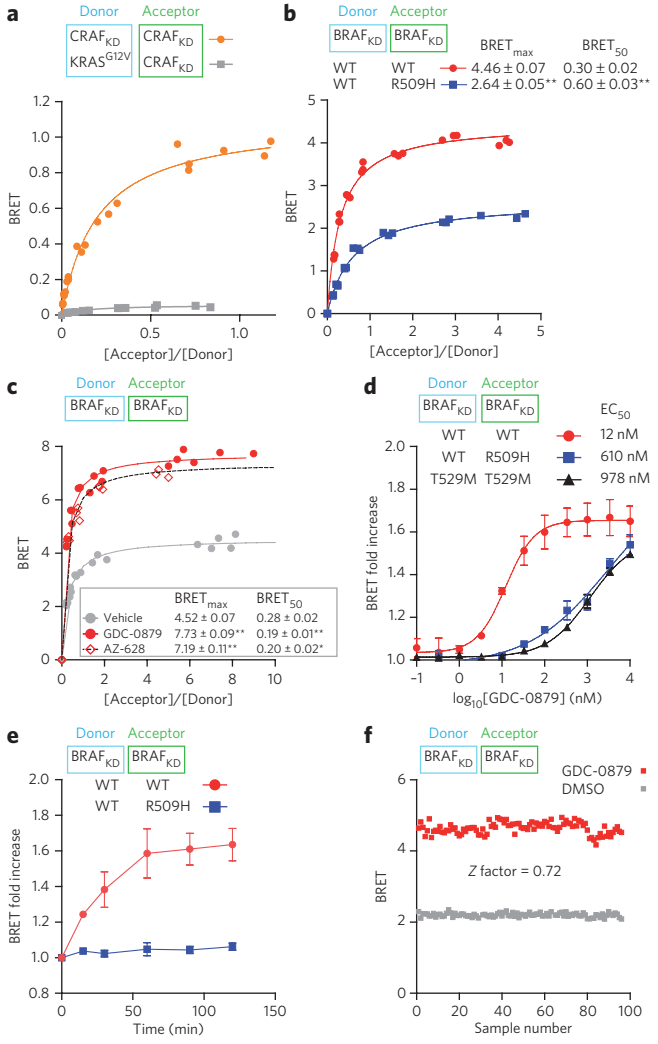

Figure 1 | Development of BRET-based RAF dimerization biosensors. (**a**) BRET titration curves of the membrane-targeted (CAAX box) $CRAF_{KD}$ biosensor. The RlucII and GFP10 moieties are inserted at the N terminus of $CRAF_{KD}$. The blue open square denotes the RlucII donor construct, whereas the green open square denotes the GFP10 acceptor construct. The noninteracting RlucII-$KRAS^{G12V}$–GFP10-$CRAF_{KD\text{-}CAAX}$ pair was used as a reference for nonspecific BRET signals. (**b**) Titration curves of wild-type (WT) versus $BRAF_{KD}^{R509H}$ BRET probes. The $BRAF_{KD}$ BRET probes used the same configuration as that shown for $CRAF_{KD}$ in **a**. The R509H mutation, which impairs side-to-side dimerization, augments $BRET_{50}$ values and reduces $BRET_{max}$ values. Double asterisks denote F-test *P* values smaller than 1×10^{-3}. (**c**) Modulation of $BRAF_{KD}$ biosensor signals upon addition (333 nM) of the indicated RAF inhibitors as assessed in titration experiments. Single asterisks denote F-test *P* values smaller than 1×10^{-3}, and double asterisks represent those smaller than 1×10^{-4}. (**d**) Mutations of the kinase domain gatekeeper residue (T529M) or the side-to-side dimerization interface (R509H) impede GDC-0879–induced BRET signals. Dose-response experiments were conducted using the indicated drug concentrations. (**e**) Induction kinetics of the $BRAF_{KD}$ BRET signal using 33 nM of GDC-0879. The R509H mutant was insensitive to the drug at this concentration. (**f**) The $BRAF_{KD}$ homodimerization BRET assay shows highly reproducible signal induction (*Z* factor = 0.72) upon GDC-0879 treatment (33 nM). Each experiment was repeated at least two times. Where error bars are presented, they correspond to mean values ± s.d. of biological triplicates.

RAF biosensors detect perturbations of dimerization

We next sought to ascertain whether the dimerization signature detected with the BRET assay depended on the side-to-side dimer interface[7,13,15]. Mutation of Arg509, which lies on the $BRAF_{KD}$ dimerization surface, was shown to reduce dimer formation and to lower kinase activity[7,17,23]. Introduction of the R509H mutation in GFP10-$BRAF_{KD}$ did not affect protein expression (**Supplementary Figs. 1d** and **2a**), but, as expected, it impeded kinase activity (**Supplementary Fig. 2a**) and reduced BRET output (**Fig. 1b**). Indeed, it significantly ($P < 0.001$) increased the $BRET_{50}$ (a proxy for affinity, which corresponds to the acceptor/donor ratio necessary to reach 50% of $BRET_{max}$) and significantly ($P < 0.001$) reduced the $BRET_{max}$ (a proxy for total number of dimers; Online Methods), which together are consistent with impaired dimer formation (**Fig. 1b**). Binding of 14-3-3 proteins to a C-terminal site on RAF proteins has been suggested to promote and/or stabilize RAF_{KD} dimer formation[7–9,24]. Consistent with this, mutagenesis of a key residue within the 14-3-3 C-terminal binding site of BRAF (S729A) significantly ($P < 0.0001$) elevated the $BRET_{50}$ and reduced ($P < 0.001$) the $BRET_{max}$ (**Supplementary Fig. 2b**).

Given the induction of RAF dimerization by specific ATP-competitive inhibitors, we examined whether the BRET assay could detect the influence of a type I (GDC-0879) and a type II inhibitor (AZ-628) that had previously been shown to promote RAF dimerization by co-immunoprecipitation[13–15]. Type I inhibitors bind their kinase target in a Asp-Phe-Gly (DFG)-in, 'active' configuration, whereas type II inhibitors bind in a DFG-out, 'inactive' configuration[25]. Consistent with the ability of the BRET assay to detect drug-induced dimer formation, both compounds significantly ($P < 0.001$) reduced the $BRET_{50}$ and augmented ($P < 0.0001$) the $BRET_{max}$ in titration experiments (**Fig. 1c**) but left total luciferase and GFP10 intensities unchanged (**Supplementary Fig. 3a**,**b**). To evaluate the potency of GDC-0879 in our system, we selected construct ratios producing $BRET_{80}$ signals (80% of $BRET_{max}$) and tested a range of GDC-0879 concentrations. A half-maximal effective concentration (EC_{50}) of 12 nM was obtained from these experiments (**Fig. 1d**), which is in the same range as the IC_{50} (34 nM) obtained by *in vitro* kinase assays[13]. To demonstrate that the compound-promoted BRET changes depended specifically on drug binding to the BRAF kinase domain, we tested the 'gatekeeper' mutation (T529M) in $BRAF_{KD}$, which reduces drug access to the catalytic cleft and prevents drug-induced RAF dimerization[15,26]. Consistent with this model, GDC-0879 increased the BRET signal with an EC_{50} 80-fold higher for $BRAF_{KD}^{T529M}$ than for the wild-type protein (**Fig. 1d**). An intact dimer interface was also required as the R509H mutation increased the EC_{50} of GDC-0879 by 50-fold (**Fig. 1d**). In agreement with previous kinetic data[13], GDC-0879 activity could be detected as early as 5 min upon drug treatment and plateaued by 60 min, whereas the R509H mutant was insensitive at the concentration tested (33 nM; **Fig. 1e**). Finally, the GDC-0879–induced BRET signal was highly reproducible and yielded a *Z* factor of 0.72 in 384-well format (**Fig. 1f**)[27]. Together, these findings indicated

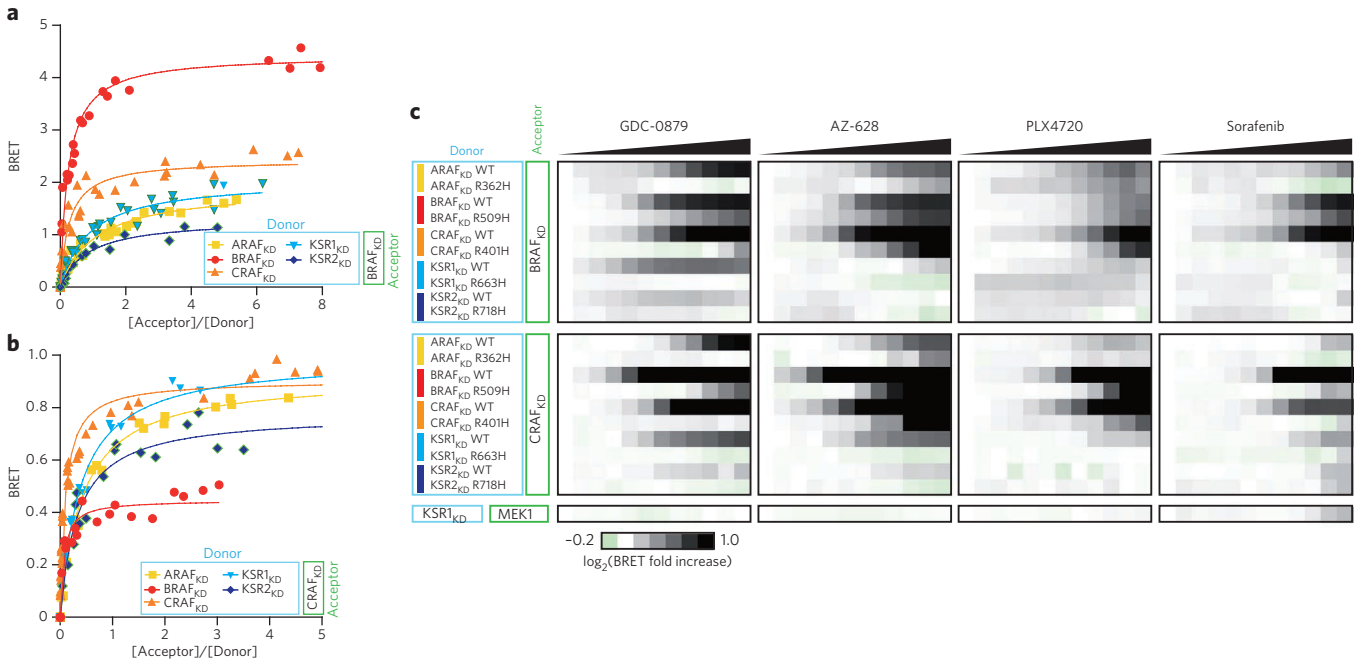

Figure 2 | Profiling RAF inhibitors using RAF dimerization biosensors. (**a**,**b**) The indicated BRET donor probes were systematically tested in titration experiments using $BRAF_{KD}$ (**a**) or $CRAF_{KD}$ (**b**) as acceptor probes. $BRET_{50}$ and $BRET_{max}$ values are shown in **Supplementary Table 1**. (**c**) Dose-response curves conducted with increasing concentrations of GDC-0879, AZ-628, PLX4720 and sorafenib (**Supplementary Fig. 5** and **Supplementary Table 2**) were log_2-transformed and converted into heat maps. Black saturation represents positive effects on BRET signals, whereas green denotes negative impacts. The residue homologous to Arg509 of BRAF was mutated in each family member and used as negative control. Each experiment was repeated at least two times.

that our BRET assay detects genuine dimerization of the RAF kinase domain *in vivo* and that it can identify compounds impinging on BRAF dimerization in a specific and sensitive manner.

RAF inhibitors distinctly affect the RAF dimer network

The ability of RAF family members to dimerize and the impact of inhibitors on dimers remain poorly understood. To investigate these issues, we generated CAAX box–containing BRET probes for the three remaining RAF family members (ARAF, KSR1 and KSR2). In contrast to the $BRAF_{KD}$ and $CRAF_{KD}$ constructs, these constructs had no substantial activity toward MEK (**Supplementary Fig. 4**). We tested all of the bidirectional pairs in titration experiments and identified GFP10-$BRAF_{KD}$ as the best BRET acceptor in terms of $BRET_{max}$ for any RAF_{KD} donor (**Fig. 2a**, **Supplementary Table 1** and data not shown). Although lower $BRET_{max}$ values were obtained with GFP10-$CRAF_{KD}$, this construct also gave robust BRET signals with each donor probe (**Fig. 2b** and **Supplementary Table 1**). In contrast, the remaining combinations gave weak and unreliable BRET signals even though the fusions were expressed to a similar degree. These observations could be explained by various reasons, such as missing factors in HEK293T cells or perturbations imposed by the GFP and/or luciferase moieties. Nevertheless, these results suggest that BRAF and CRAF have the capacity to engage in dimer formation with any member of the RAF family. Finally, distinct $BRET_{max}$ and $BRET_{50}$ values were observed for each pair. Although these parameters are useful for comparing the dimerization potential of a given pair as a consequence of amino acid changes or upon drug treatment (**Fig. 1**), they cannot be used to compare altogether different pairs.

Using the full donor panel of RAF biosensors, we verified whether other dimers could form upon drug treatment and thus predict their occurrence *in vivo*. We evaluated the impact of GDC-0879, AZ-628 and two other RAF inhibitors, namely PLX4720 (a type I inhibitor[28]) and sorafenib (a type II inhibitor[29]), on each RAF_{KD} pair using the $BRAF_{KD}$ and $CRAF_{KD}$ acceptor probes (**Fig. 2c**, **Supplementary Fig. 5a**,**b** and **Supplementary Table 2**). Remarkably, the inhibitors showed distinct induction profiles that depended on an intact dimer interface (**Fig. 2c**). Further demonstrating the specificity of the effect, the four compounds did not modulate an unrelated interacting pair (**Fig. 2c** and **Supplementary Fig. 5c**,**d**). PLX4720 and sorafenib were relatively weak RAF_{KD} dimer inducers (summarized in **Supplementary Fig. 6a**). In contrast, both GDC-0879 and AZ-628 were strong and broad inducers of BRAF-containing dimers, and yet, each showed differences in their ability to promote specific RAF dimers. Notably, whereas GDC-0879 strongly induced BRAF-KSR1 dimers, AZ-628 did not. Conversely, AZ-628 (but not GDC-0879) strongly promoted CRAF homodimers. To rule out the possibility that BRET signal variations reflected protein conformational changes rather than dimerization, we conducted titration experiments on three pairs, namely $ARAF_{KD}$–$BRAF_{KD}$, $CRAF_{KD}$–$BRAF_{KD}$ and $KSR1_{KD}$–$BRAF_{KD}$, with or without drug treatment. In every case, we observed a significant ($P < 0.001$) reduction of the $BRET_{50}$ value, supporting the notion that the inhibitors promoted RAF dimer formation (**Supplementary Fig. 6b–d**). Together, these data suggest that RAF inhibitors modulate the dimerization landscape of the RAF family in a complex and selective manner. Differences in induction profiles most likely reflect differences in (i) compound affinity for and structural impact on RAF proteins, (ii) compound pharmacokinetics and (iii) the inherent propensity of RAF dimerization surfaces to pair among themselves.

RAF_{KD} biosensors behave as RAS-induced full-length RAF

The induction of RAF dimerization by kinase inhibitors was shown to depend on RAS activity[13–15]. We were thus intrigued that our CAAX-boxed RAF_{KD} biosensors could detect dimerization in the absence of overt RAS activity. We reasoned that the CAAX box on our RAF_{KD} biosensors mimicked the recruitment of RAF to the plasma membrane triggered by RAS activation[2]. Moreover, RAS binding to RAF is

thought to release an inhibitory interaction between the N-terminal regulatory region of RAF and the kinase domain, enabling kinase domain dimerization[2]. By using isolated kinase domains, the propensity of our biosensors to dimerize would therefore be increased, thereby bypassing the need for upstream inputs.

To verify whether our RAF_{KD} biosensors simulate a RAS-mediated context, we generated full-length (FL) BRAF and CRAF BRET biosensors and characterized their ability to form dimers in a RAS-dependent manner and compared their dimerization profiles upon RAF inhibitor treatment. In the absence of co-expressed RAS^{G12V}, the $CRAF_{FL}$–$BRAF_{FL}$ pair produced titration curves that fit a low-confidence hyperbolic function, suggestive at best of weak dimerization (**Fig. 3a** and **Supplementary Table 3**). In contrast, expression together with mCherry-tagged activated KRAS ($KRAS^{G12V}$ or $KRAS^{Q61H}$) strongly stimulated $CRAF_{FL}$–$BRAF_{FL}$ dimerization in a dose-dependent manner (**Fig. 3a** and **Supplementary Fig. 7**). Demonstrating the specificity of the RAF_{FL} dimerization assay, a dominant-negative $KRAS^{S17N}$ and a RAF RBD mutation (R188L) in BRAF did not support $CRAF_{FL}$–$BRAF_{FL}$ dimerization (**Fig. 3a**). In addition, the R509H mutation in the BRAF side-to-side interface weakened dimerization, as evidenced by an increased $BRET_{50}$ value (**Fig. 3a** and **Supplementary Table 3**).

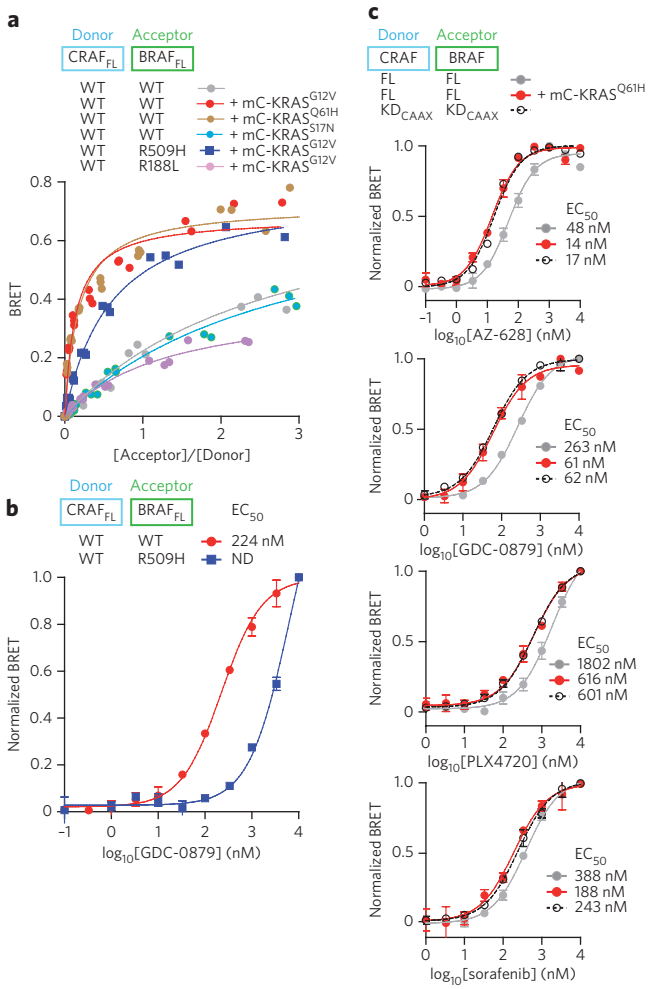

Figure 3 | Development of a RAS-dependent CRAF-BRAF dimerization biosensor. (**a**) Titration experiment using $CRAF_{FL}$ donor (RlucII) probe and wild-type BRAF or mutant $BRAF_{FL}$ acceptor (GFP10) probe with or without mCherry (mC)-tagged $KRAS^{G12V}$, $KRAS^{Q61H}$ or $KRAS^{S17N}$. The mCherry tag was used for monitoring KRAS expression. Its excitation and emission spectra do not overlap with those of our BRET donor or acceptor constructs[20]. $BRET_{50}$ and $BRET_{max}$ values are shown in **Supplementary Table 3**. (**b**) Drug-induced BRET signals for the $CRAF_{FL}$-$BRAF_{FL}$ biosensor depend on an intact dimerization interface. ND, not determined. (**c**) Co-expression of mCherry-tagged $KRAS^{Q61H}$ potentiates drug-induced dimerization, as measured by a decrease in the EC_{50} for each RAF inhibitor tested. Dose-response experiments with the indicated RAF inhibitors on the CAAX-boxed $CRAF_{KD}$-$BRAF_{KD}$ biosensor produced EC_{50} values nearly identical to those obtained with the RAS-induced $CRAF_{FL}$-$BRAF_{FL}$ biosensor. Because of their distinct intensities (for instance, biosensors in the presence of co-expressed $KRAS^{Q61H}$ yield higher signals), BRET signals were normalized from 0 (vehicle-treated cells) to 1.0 (maximal effect of a given compound). This facilitated the comparison of the response of distinct BRET pairs to specific compounds. Each experiment was repeated at least two times. Where error bars are presented, they correspond to mean values ± s.d. of biological triplicates.

We next conducted RAF inhibitor dose-response experiments on the $CRAF_{FL}$ and $BRAF_{FL}$ probes with and without RAS and compared the responses to those obtained with the $CRAF_{KD}$–$BRAF_{KD}$ biosensors. Markedly, each inhibitor induced the $CRAF_{FL}$–$BRAF_{FL}$ BRET signals in the absence of coexpressed RAS (**Fig. 3b**,**c**), suggesting that basal RAS activity in HEK293T cells supports drug-induced $CRAF_{FL}$–$BRAF_{FL}$ dimerization. Alternatively, it is possible that the compounds promote full-length RAF dimerization in a RAS-independent manner, a phenomenon not detected previously that is possibly due to the low sensitivity of dimerization detection methods used. At any rate, the induction was dependent on a functional side-to-side interface because the R509H mutation in the $BRAF_{FL}$ probe increased the EC_{50} of the $CRAF_{FL}$ and $BRAF_{FL}$ biosensors to GDC-0879 by approximately 30-fold (**Fig. 3b**). Notably, constitutive RAS activity systematically reduced the EC_{50} of each compound for the $CRAF_{FL}$–$BRAF_{FL}$ pair to an extent that is nearly identical to that obtained with the $CRAF_{KD}$–$BRAF_{KD}$ probes (**Fig. 3c**), consistent with the notion that the N-terminal region of RAF represses the dimerization potential of the kinase domain in the absence of RAS activity. Together, these findings further support the importance of RAS function for the ability of RAF inhibitors to promote RAF dimerization and provide evidence that our CAAX-boxed RAF_{KD} biosensors mimic a RAS-induced state.

A screen for modulators of CRAF–BRAF dimers

We exploited the robustness and scalability of our RAF dimerization assay in a high-throughput screen to identify compounds that selectively modulate RAF dimerization. We selected the $CRAF_{KD}$–$BRAF_{KD}$ biosensor pair and screened a library of ~115,000 small molecules assembled primarily from commercial sources. Compounds affecting RlucII luminescence or intrinsic GFP10 fluorescence by greater than two-fold were not considered further. We identified 503 primary hits (249 activators and 254 inhibitors) using a cutoff of 3 s.d. from controls (**Fig. 4a**). Retesting confirmed 47% of the hits. Two alternate BRET-based interaction assays ($KSR1_{KD}$–MEK1 and $KRAS^{G12V}$–$BRAF_{FL}$) were then carried out to narrow down the list of hits to molecules selective for the $CRAF_{KD}$–$BRAF_{KD}$ biosensor. Doing so eliminated ~70% of the primary hits, resulting in 8 inducers and 65 suppressors of dimerization.

We initially focused our attention on the most potent inducer, UM0119603 (**Fig. 4a**,**b**). This compound, also known as SB202190, was developed as a specific ATP-competitive inhibitor of p38 MAPK[30] (**Supplementary Figs. 8** and **9**). Notably, a close structural analog (SB203580; **Supplementary Fig. 8**) was previously recognized as a p38-independent inducer of RAF activity[31,32], but the mechanism of action was not known. The identification of SB202190 as an inducer of the $CRAF_{KD}$–$BRAF_{KD}$ BRET signal suggested that this class of molecules stimulates RAF by promoting dimerization. Consistent with this notion, SB203580 also induced the $CRAF_{KD}$–$BRAF_{KD}$ BRET signal, and both SB203580 and SB202190 required an intact RAF dimerization surface to show an effect (**Fig. 4c**). The higher EC_{50}

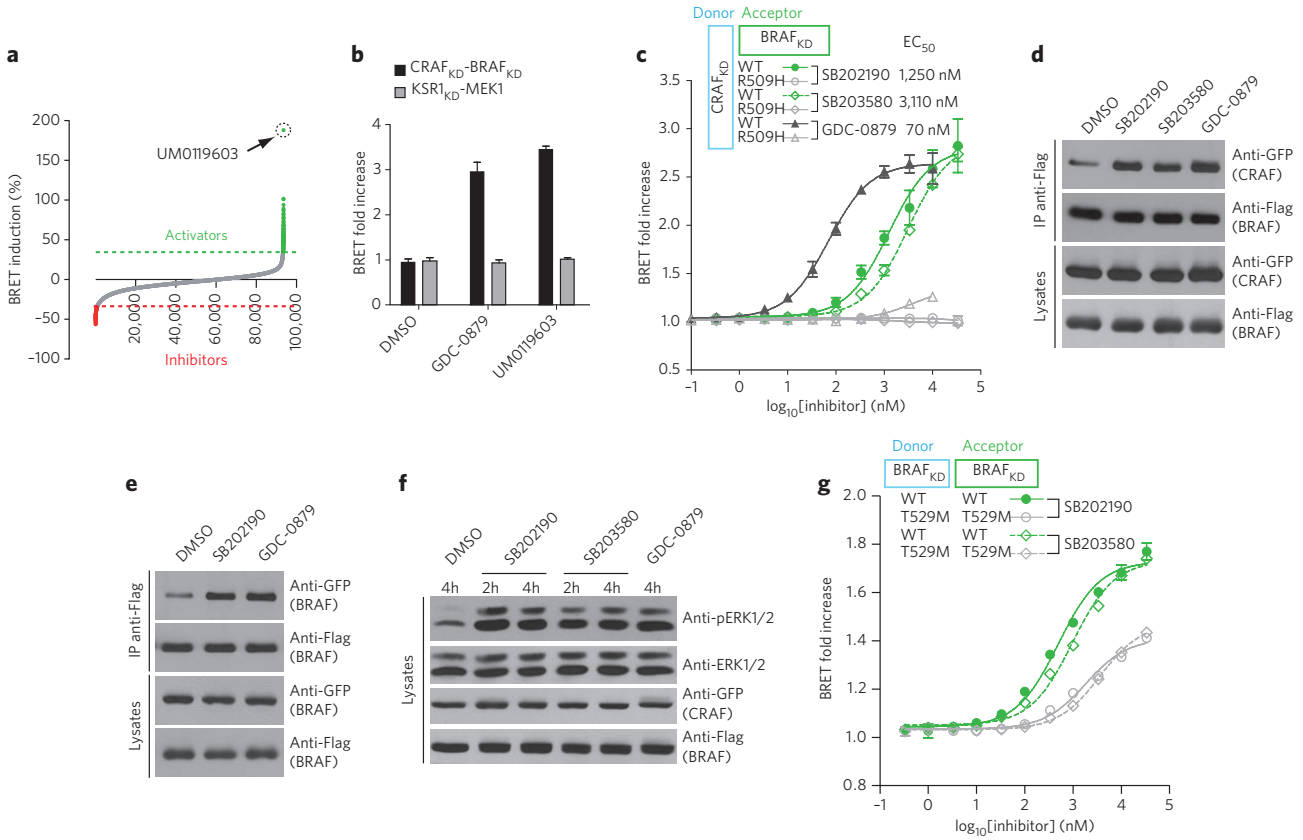

Figure 4 | A high-throughput chemical screen using the CRAF$_{KD}$–BRAF$_{KD}$ biosensor identifies new modulators of RAF dimerization. (**a**) Distribution of the compound activities in a high-throughput screen performed on ~115,000 drug-like compounds. UM0119603 was the most potent inducer of CRAF$_{KD}$–BRAF$_{KD}$ dimerization. (**b**) Like GDC-0879, UM0119603 induces the CRAF$_{KD}$–BRAF$_{KD}$ BRET signal (10 μM), but it does not alter the BRET produced by the KSR1$_{KD}$–MEK1 pair. (**c**) Dose-response experiments performed with a range of SB202190 and SB203580 concentrations. Mutations of the side-to-side dimerization interface (R509H) abolished the effect of each inhibitor. GDC-0879 was used as an internal standard. EC$_{50}$ value calculated for each compound is shown. WT, wild type. (**d**,**e**) The two p38 inhibitors (SB202190 and SB203580) induce the formation of full-length BRAF–CRAF and BRAF–BRAF dimers, as demonstrated by co-immunoprecipitation (co-IP) (SB202190 and SB203580, 10 μM; GDC-0879, 1 μM). Anti-Flag, antibody to Flag. (**f**) p38 inhibitors induce ERK phosphorylation in RAF-expressing HEK293T cells (SB202190 and SB203580, 2 μM; GDC-0879, 1 μM). (**g**) Dose-response experiments show that a T529M gatekeeper mutant of BRAF reduces BRAF$_{KD}$ homodimerization induced either by SB202190 or SB203580. Each experiment was repeated at least two times. Where error bars are presented, they correspond to mean values ± s.d. of biological triplicates.

values of SB203580 and SB202190 compared to that of GDC-0879 most likely reflect their weaker affinity for RAF proteins. To further validate their capacity to promote RAF dimerization, we conducted co-immunoprecipitation experiments using full-length GFP-CRAF and Flag-BRAF. Both SB203580 and SB202190 increased BRAF–CRAF dimerization in a manner comparable to GDC-0879 stimulation (**Fig. 4d**). The effect of the compounds was not restricted to CRAF–BRAF heterodimers as SB202190 also induced BRAF homodimerization (**Fig. 4e**). Finally, consistent with their ability to promote dimerization, both compounds stimulated ERK activity in RAF-transfected cells (**Fig. 4f**).

We noticed a marked structural similarity between SB202190, SB203580 and two other RAF inhibitors, L779450 and SB590885, which were previously shown to induce RAF dimerization[14,33] (**Supplementary Fig. 8**). The binding mode of SB590885 in the catalytic cleft of BRAF[34] shows the same general orientation and conformation as its structural analog SB203580 in its co-crystal with the p38 MAP kinase[35] (**Supplementary Fig. 8b**,**c**). This implies that the p38 inhibitors may interact with RAF in a manner similar to their interaction with p38. Given their predicted binding mode in the BRAF catalytic cleft, we surmised that the gatekeeper mutation would impair their binding and thereby weaken their ability to induce RAF dimerization. Indeed, the BRAF$_{KD}^{T529M}$ biosensor pair had an EC$_{50}$ roughly four times higher for the two p38 inhibitors than that of the wild type (**Fig. 4g**). These data provide compelling evidence that our biosensors can identify selective RAF dimerization modulators from compound libraries and that p38 inhibitors selectively induce RAF dimerization and downstream signaling in a manner related to known RAF inhibitors.

Diverse kinase inhibitors induce RAF dimerization

The observation that two p38 inhibitors can induce RAF dimerization prompted us to investigate the effect of other ATP-competitive kinase inhibitors on our panel of RAF dimer biosensors. We assembled a collection of 184 compounds targeting a broad spectrum of kinases, most of which had been profiled for inhibition of *in vitro* kinase activity against approximately 300 kinases, including RAF proteins[36]. Our analysis identified several compounds that reproducibly induced dimerization as measured by BRET (**Fig. 5a** and **Supplementary Data Set 1**). In general, the dimer-inducing activity of the kinase inhibitors correlated with their reported ability to inhibit the *in vitro* kinase activity of BRAF or CRAF (**Fig. 5a** and **Supplementary Data Set 1**). Notably, in addition to retrieving all of the RAF inhibitors present in the library, we identified multiple inhibitors of three distinct kinases, namely six inhibitors of p38, three inhibitors of BCR-ABL and four inhibitors of VEGFR, as

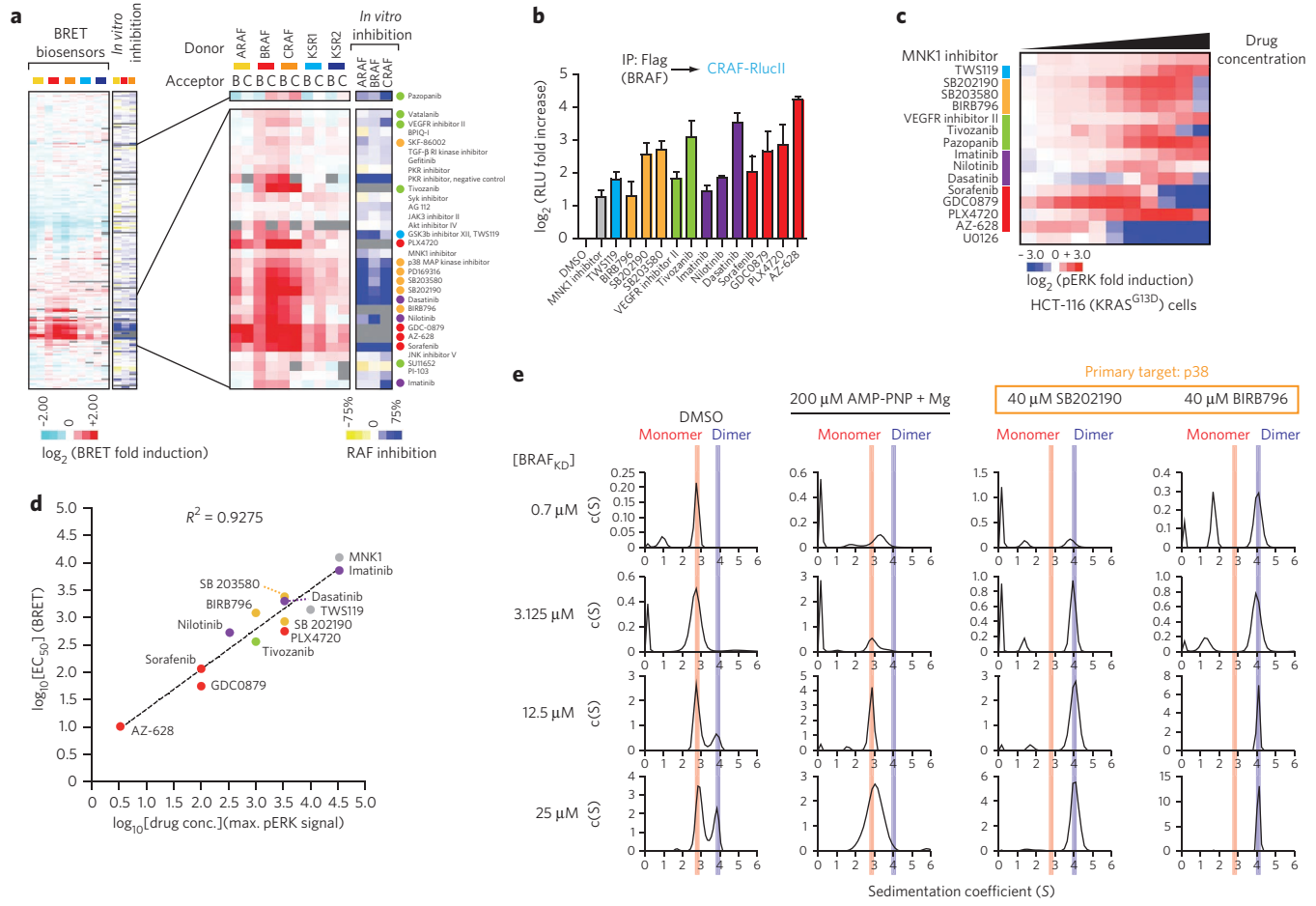

Figure 5 | Screening of a kinase inhibitor library reveals widespread off-target effects on RAF dimerization. (**a**) Unsupervised clustering of the response of a panel of RAF dimerization BRET biosensors tested against a library of kinase inhibitors (left panel; **Supplementary Data Set 1**). For comparison, a heat map depicting previously published *in vitro* RAF kinase inhibition[36] is shown. Gray bars denote data not available. The right panel shows enlarged areas comprising BRET inducers. (**b**) Confirmation of the dimerization-inducing potential of selected kinase inhibitors. Flag-BRAF was expressed together with CRAF-RlucII, and luciferase activity was monitored in Flag-specific antibody (anti-Flag) immunoprecipitates (IPs). Data were from triplicates and normalized to data from DMSO treatment. Error bars correspond to s.d. (**c**) HCT-116 cells were treated (2 h) with increasing concentrations of the indicated compounds. The amount of pERK (**Supplementary Fig. 11**) was normalized to that in cells treated with DMSO, $\log_2$-transformed and converted into heat maps. (**d**) Correlation between concentrations causing maximal amounts of pERK (**Fig. 5c** and **Supplementary Fig. 11**) and the BRET EC_{50} values for the same compounds against the $CRAF_{KD}$–$BRAF_{KD}$ pair (**Supplementary Fig. 10b**). (**e**) Analytical ultracentrifugation demonstrates the ability of type I and type II p38 inhibitors to promote $BRAF_{KD}$ dimerization *in vitro*. AMP-PNP inhibits $BRAF_{KD}$ dimerization. The positions of monomeric and dimeric $BRAF_{KD}$ are indicated by red and blue lines, respectively. Peaks at or below 2 Svedbergs (S) represent artifacts of the refractive index detector system that is evident at low protein concentrations. Peak heights are not dependent on protein concentration. c(S) denotes sedimentation coefficient distribution.

likely inducers of RAF dimerization (**Fig. 5a** and **Supplementary Figs. 9** and **10**). Supporting our findings, the same three BCR-ABL inhibitors (imatinib, nilotinib and dasatinib) were reported to promote RAF dimerization in co-immunoprecipitation assays and to stimulate ERK signaling in leukemic cells[37].

To establish that the BRET-inducing kinase inhibitors genuinely promoted RAF dimerization, we evaluated the activity of the 14 strongest inhibitors (**Supplementary Fig. 9**) in co-immunoprecipitation experiments using the luminescence-based mammalian interactome mapping (LUMIER) assay[38]. As shown in **Figure 5b**, all inhibitors promoted BRAF-CRAF co-immunoprecipitation. Moreover, as predicted from their RAF-dimerizing properties, the same compounds induced ERK phosphorylation in $KRAS^{G13D}$ mutant cells (HCT-116; **Fig. 5c** and **Supplementary Fig. 11**) but reduced ERK activation in wild-type KRAS and $BRAF^{V600E}$ mutant cells (COLO205; **Supplementary Fig. 11**). We observed a strong correlation between the concentration of inhibitor causing maximal ERK activation and its associated $CRAF_{KD}$–$BRAF_{KD}$ BRET EC_{50} (**Fig. 5d**). To verify that the BRET-inducing kinase inhibitors acted by direct binding to the RAF catalytic cleft, we used an *in vitro* time-resolved (TR)-FRET–based assay to monitor the ability of the compounds to compete with a fluorescent kinase tracer bound to the BRAF orthosteric site. All of the compounds with off-target effects on RAF dimerization effectively displaced the tracer (**Supplementary Fig. 12**). Notably, with the exception of PLX4720, the IC_{50} values for these inhibitors closely correlated with their EC_{50} values in the $BRAF_{KD}$–$BRAF_{KD}$ BRET assay, suggesting that the BRET assay can also predict the affinity of small-molecule inhibitors for RAF (**Supplementary Fig. 12f**).

Kinase inhibitors induce RAF dimerization *in vitro*

To test whether induced dimerization was mediated directly by the kinase domain of RAF as a consequence of inhibitor binding, we established a sedimentation velocity analytical ultracentrifugation (AUC) assay using the purified BRAF kinase domain. We first characterized the isolated kinase domain of human BRAF (residues 444 to 723) in

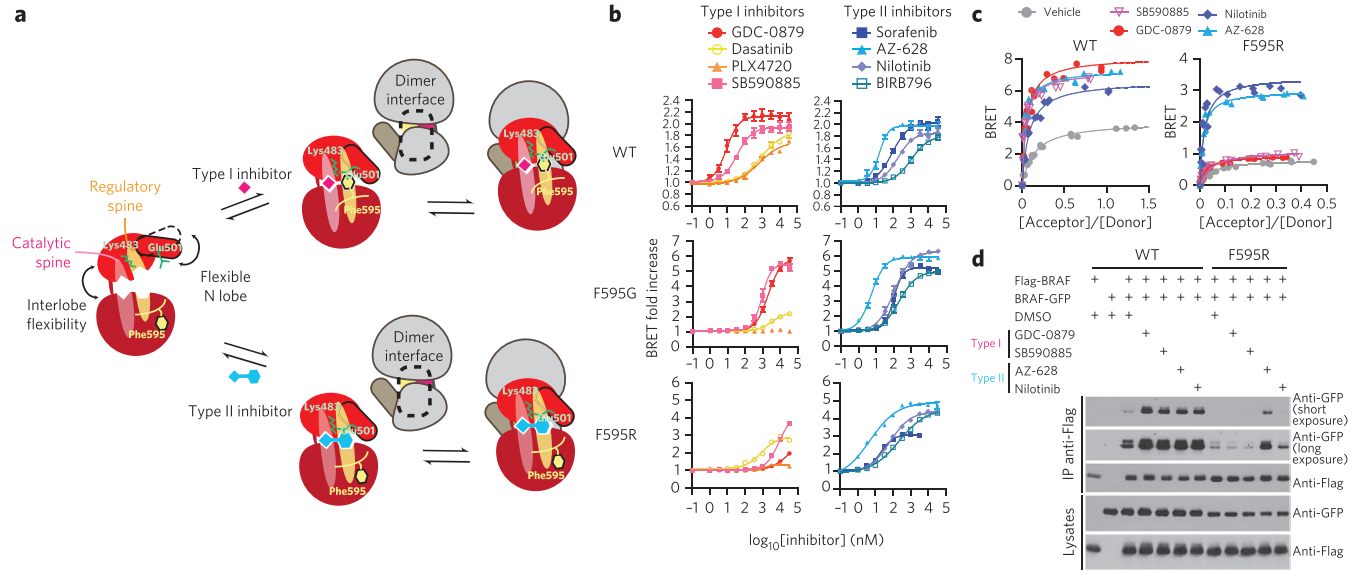

Figure 6 | Probing the binding mode of RAF dimer inducers with BRAF mutant biosensors. (**a**) Models for type I (top) and type II (bottom) kinase inhibitor–induced RAF dimerization. (**b**) $BRAF_{KD}$ regulatory spine (F595R or F595G) mutants can distinguish type I from type II inhibitors by the capacity of the latter to selectively induce the dimerization of regulatory spine mutant variants as monitored by BRET. WT, wild type. (**c**) BRET saturation curves also demonstrate the distinct ability of type II inhibitors (AZ-628 and nilotinib) over type I inhibitors (GDC-0879 and SB590885) to promote dimerization of a BRAF regulatory spine mutant (F595R). (**d**) Co-immunoprecipitation (co-IP) of full-length $BRAF^{F595R}$ is selectively induced by type II but not by type I inhibitors. Each experiment was repeated at least two times. Where error bars are presented, they correspond to mean values ± s.d. of biological triplicates.

its apo state and found a weak ability to dimerize with a K_d greater than 25 μM (**Fig. 5e** and **Supplementary Fig. 13**). This was considerably weaker than that observed previously for a shorter BRAF kinase domain construct (residues 448 to 723, K_d < 6.25 μM) analyzed by sedimentation equilibrium[7] and may reflect either a real difference in dimerization propensity or a difference in experimental conditions.

We then tested the impact of GDC-0879 at saturating inhibitor concentration (40 μM)[13]. We observed a substantial enhancement in the ability to form dimers (K_d <<< 0.78 μM) such that no evidence of a monomer state was observed, even at the lowest detectable concentration of BRAF protein (0.78 μM) (**Supplementary Fig. 13**). Analysis of the RAF inhibitor AZ-628 revealed a similar enhancement of dimerization (K_d <<< 0.78 μM) (**Supplementary Fig. 13**) as did sorafenib, but the limited solubility of sorafenib in aqueous solution hampered a comparable full analysis (data not shown).

We next examined the effect of other kinase inhibitors predicted by BRET to have off-target effects on RAF dimerization. Consistent with their effects on BRET, SB202190, BIRB796, dasatinib, nilotinib and tivozanib enhanced dimerization relative to the apo state (**Fig. 5e** and **Supplementary Fig. 13**). Remarkably, ADP and the ATP mimetic AMP-PNP, in contrast, inhibited dimer formation with no dimer species detected even at the highest protein concentration tested (25 μM; **Fig. 5e** and **Supplementary Fig. 13**). Together, these findings demonstrate that kinase inhibitors promote RAF dimerization directly through effects on the kinase domain.

Model for inhibitor-induced RAF dimerization

Available co-structures for RAF dimer–promoting kinase inhibitors bound to RAF or to other protein kinase domains (**Supplementary Figs. 9** and **14**) did not reveal any obvious feature in either small-molecule structure or binding mode that could readily explain why these diverse molecules commonly promote RAF dimerization. The only comparable characteristic of all of the co-structures was that the kinase domains adopted a closed conformation of the N and C lobes. Protein kinases are dynamic, with a large degree of flexibility between N and C lobes and within the N lobe itself (**Fig. 6a**). With respect to the latter, helix αC is tenuously tethered to a five strand β-sheet, which provides great opportunity for regulatory control of phosphotransfer function[39,40]. Notably, the side-to-side dimerization surface of RAF kinases spans both N and C lobes[7] (**Fig. 6a**). Furthermore, the N lobe portion of the contact surface spans both the β-sheet and helix αC components. Thus, dimerization through the side-to-side surface would require a great restriction in flexibility of the RAF kinase domain. We posited that the binding of dimer-promoting compounds to the catalytic cleft of the RAF kinase domains, irrespective of their variable modes of association, commonly stabilize the kinase domain in the closed state, thereby promoting dimerization.

The alignment of the hydrophobic regulatory and catalytic spines, each of which traverses both N and C lobes of the kinase domain, serves as a diagnostic feature of low-energy closed conformations of the kinase domain[41,42] (**Fig. 6a** and **Supplementary Figs. 14** and **15**). All of the inhibitors found to induce RAF dimerization preserve spine alignment (**Supplementary Fig. 14**) through related but distinct mechanisms. Type I inhibitors achieve spine alignment by binding within the ATP-binding pocket to bridge the N and C lobes along the catalytic spine (**Fig. 6a** and **Supplementary Fig. 15**). The regulatory spine, in contrast, is composed strictly of hydrophobic side chains of the kinase domain, including the phenylalanine of the DFG motif. Type II inhibitors bind the ATP-binding pocket and similarly bridge the N and C lobes along the C spine but also occupy the DFG-out hydrophobic pocket (as a surrogate phenylalanine) to directly bridge the N and C lobes along the regulatory spine (**Fig. 6a** and **Supplementary Fig. 15**). The end result of either inhibitor-binding mode is a closed rigid conformation of the kinase domain that presents a relatively static outer surface conducive to dimerization.

If lobe closure is essential for creating a productive dimerization interface, we hypothesized that interfering with it should reduce dimerization. To verify this, we mutagenized the DFG phenylalanine (Phe595) in BRAF to a glycine or arginine, as these changes have

been reported to induce a constitutive DFG-out–like conformation in p38α[43]. Consistent with our model, DFG mutant $BRAF_{KD}$ biosensors showed an important reduction in dimerization-dependent BRET signals (**Supplementary Fig. 16a**), and similar loss of dimerization was observed by co-immunoprecipitation (**Fig. 6**).

To further test the model, we took advantage of the distinct binding modes of type I and type II inhibitors (schematized in **Supplementary Fig. 16b**). Type I inhibitors should be sensitive to DFG mutations as the DFG-in configuration is unattainable with such mutations. In addition, their affinity for DFG mutants might be reduced as type I inhibitors are selected on the basis of their binding to DFG-in configurations. In contrast, given that type II inhibitors provide a surrogate phenylalanine, they should bind DFG mutants similarly to the wild type and promote a closed configuration, enabling dimerization. We first tested the binding of both classes of inhibitors by TR-FRET, and indeed our predictions were confirmed (**Supplementary Fig. 16c**,**d**). Next, we examined the ability of both classes to promote dimerization of wild-type versus DFG BRAF mutants. As shown in **Figure 6b**, four distinct type I inhibitors were highly sensitive to DFG mutations, whereas four type II inhibitors were less so (**Supplementary Table 4**). Co-crystal structures confirmed that BIRB796 bound BRAF in a DFG-out conformation (**Supplementary Fig. 17** and **Supplementary Table 5**). We then characterized two representative inhibitors from each class for dimerization potential using BRET titration and BRAF co-immunoprecipitation assays (**Fig. 6c**,**d**). Again we observed that type I inhibitors were more sensitive to the DFG mutation than type II inhibitors. Together, these findings are consistent with a model whereby kinase inhibitors promote RAF dimerization by stabilizing a rigid closed conformation of the kinase domain.

PERK kinase domain shows inhibitor-induced dimerization

We next examined whether other protein kinase families regulated by kinase domain dimerization would respond similarly to the binding of kinase inhibitors. Recently, a nanomolar inhibitor, GSK2606414, was reported for PERK[44], a member of the eIF2α kinase family that is regulated through a distinct mode of dimerization[45,46]. Crystallographic analysis revealed a type I inhibitor-binding mode with unconventional features resembling a type II inhibitor-binding mode[44]. Indeed, although the DFG-out allosteric binding pocket remained occupied by DFG, GSK2606414 displaces another catalytic spine residue, Leu642. Nevertheless, contacts between the lobes are still maintained along the catalytic spine through GSK2606414, allowing a rigid closed conformation that we reasoned would favor dimerization in solution, as observed in the crystal environment. AUC analysis showed that the apo form of PERK was predominantly a monomer at all of the kinase domain concentrations tested (**Supplementary Fig. 18**). Saturating concentrations of ADP weakly promoted dimerization, whereas saturating concentrations of a close structural analog of GSK2606414 (ref. 47) strongly promoted dimerization. Because the mode of dimerization of the eIF2α kinase and RAF family kinases are entirely unrelated and the inhibitors that promote RAF and PERK dimer formation are chemically distinct, these results support the notion that dimer-promoting inhibitors may act through a common ability to restrict kinase domain dynamics.

DISCUSSION

The observation that dimerization is critical for RAF activation and that ATP-competitive inhibitors exert paradoxical effects by stimulating RAF dimerization has raised caution regarding their clinical use and has created a need for methods enabling fast and reliable detection of RAF dimerization. The BRET-based assay presented here offers high sensitivity and reproducibility as well as quantitative real-time monitoring of RAF dimerization in living cells. The flexibility and simplicity of the assay make possible exhaustive surveys aimed at characterizing the dimerization properties of any RAF family member combination under a vast range of conditions and enables assessment of how mutations or small molecules impinge on RAF activity.

Despite the high conservation across RAF kinase domain isoforms, our data show that kinase inhibitors can exert selective effects on their dimerization. This underscores the need to assess the overall impact of lead compounds on the RAF dimerization landscape to minimize unanticipated adverse biological consequences. Moreover, in addition to bona fide RAF inhibitors, our data and those from other groups[37,48] indicate that other kinase inhibitors can modulate RAF oligomeric status and thereby influence RAF activity. This would argue for a need to assess the RAF dimer–inducing potential of all of the kinase inhibitors in development for therapeutic use.

In contrast to the effect of protein kinase inhibitors, we found that ADP and AMP-PNP inhibit BRAF dimerization relative to the weakly dimerizing apo state. Consistent with these findings, previous work also observed reduced BRAF–CRAF interaction by co-immunoprecipitation on purified proteins in the presence of an ATP analog[13]. Although structures of dimer-promoting inhibitors bound to BRAF or CRAF are plentiful, structures bound to nucleotide and/or structures of RAF in a monomeric state are still lacking. This might reflect the fact that ATP and ADP binding to RAF disfavors the side-to-side dimer configuration. One possible explanation for this unexpected difference is that the binding mode of nucleotides precludes a rigid clamping of the kinase domain. If true, this might reflect the importance of conformational dynamics in the catalytic mechanism of phosphotransfer. A second possibility relates to the issue of affinity. ATP and ADP binding affinity to active state kinase domains typically lies in the micromolar range, whereas inhibitors commonly bind their targets in the picomolar to nanomolar range. By selecting for high binding affinity, kinase inhibitors might be inescapably better at rigidifying the kinase domain, hence promoting RAF dimerization. This could suggest that it may be difficult to optimize inhibitor affinity independent of dimer-promoting ability. If true, one possible solution would be to identify inhibitors that induce a rigid conformation of the kinase domain but specify one that is sufficiently distorted to preclude dimerization. Alternatively, it may be possible to engineer high-affinity inhibitors that do not restrict the intrinsic flexibility of the kinase domain by binding sites remote from the catalytic cleft. An obvious site would be the dimer interface itself.

Like the RAF family, the eIF2α kinases (PERK, GCN2, PKR and HRI) are also regulated through a dimer-induced allosteric mechanism[45,46,49]. We have shown that the PERK-specific inhibitor GSK2606414 potently promotes PERK kinase domain dimerization. Whether GSK2606414 binding to PERK can promote the formation of active heterodimers between PERK and GCN2, PKR or HRI remains to be determined. Given the unintended consequences of RAF kinase inhibitors currently in clinical use, it would be advantageous to verify this possibility for all of the protein kinase families regulated by kinase domain dimerization.

Received 19 November 2012; accepted 17 April 2013;
published online 19 May 2013

METHODS

Methods and any associated references are available in the online version of the paper.

Accession codes. Protein Data Bank (PDB): the coordinates for BRAF-BIRB796 have been submitted under accession code 4JVG.

References

1. Roberts, P.J. & Der, C.J. Targeting the Raf-MEK-ERK mitogen-activated protein kinase cascade for the treatment of cancer. *Oncogene* **26**, 3291–3310 (2007).

2. Wellbrock, C., Karasarides, M. & Marais, R. The RAF proteins take centre stage. *Nat. Rev. Mol. Cell Biol.* **5**, 875–885 (2004).
3. Dhomen, N. & Marais, R. New insight into BRAF mutations in cancer. *Curr. Opin. Genet. Dev.* **17**, 31–39 (2007).
4. Schubbert, S., Shannon, K. & Bollag, G. Hyperactive Ras in developmental disorders and cancer. *Nat. Rev. Cancer* **7**, 295–308 (2007).
5. Clapéron, A. & Therrien, M. KSR and CNK: two scaffolds regulating RAS-mediated RAF activation. *Oncogene* **26**, 3143–3158 (2007).
6. Garnett, M.J., Rana, S., Paterson, H., Barford, D. & Marais, R. Wild-type and mutant B-RAF activate C-RAF through distinct mechanisms involving heterodimerization. *Mol. Cell* **20**, 963–969 (2005).
7. Rajakulendran, T., Sahmi, M., Lefrancois, M., Sicheri, F. & Therrien, M. A dimerization-dependent mechanism drives RAF catalytic activation. *Nature* **461**, 542–545 (2009).
8. Rushworth, L.K., Hindley, A.D., O'Neill, E. & Kolch, W. Regulation and role of Raf-1/B-Raf heterodimerization. *Mol. Cell Biol.* **26**, 2262–2272 (2006).
9. Weber, C.K., Slupsky, J.R., Kalmes, H.A. & Rapp, U.R. Active Ras induces heterodimerization of cRaf and BRaf. *Cancer Res.* **61**, 3595–3598 (2001).
10. Halilovic, E. & Solit, D.B. Therapeutic strategies for inhibiting oncogenic BRAF signaling. *Curr. Opin. Pharmacol.* **8**, 419–426 (2008).
11. Bollag, G. *et al.* Clinical efficacy of a RAF inhibitor needs broad target blockade in BRAF-mutant melanoma. *Nature* **467**, 596–599 (2010).
12. Joseph, E.W. *et al.* The RAF inhibitor PLX4032 inhibits ERK signaling and tumor cell proliferation in a V600E BRAF-selective manner. *Proc. Natl. Acad. Sci. USA* **107**, 14903–14908 (2010).
13. Hatzivassiliou, G. *et al.* RAF inhibitors prime wild-type RAF to activate the MAPK pathway and enhance growth. *Nature* **464**, 431–435 (2010).
14. Heidorn, S.J. *et al.* Kinase-dead BRAF and oncogenic RAS cooperate to drive tumor progression through CRAF. *Cell* **140**, 209–221 (2010).
15. Poulikakos, P.I., Zhang, C., Bollag, G., Shokat, K.M. & Rosen, N. RAF inhibitors transactivate RAF dimers and ERK signalling in cells with wild-type BRAF. *Nature* **464**, 427–430 (2010).
16. Poulikakos, P.I. & Rosen, N. Mutant BRAF melanomas—dependence and resistance. *Cancer Cell* **19**, 11–15 (2011).
17. Poulikakos, P.I. *et al.* RAF inhibitor resistance is mediated by dimerization of aberrantly spliced BRAF(V600E). *Nature* **480**, 387–390 (2011).
18. Solit, D.B. & Rosen, N. Resistance to BRAF inhibition in melanomas. *N. Engl. J. Med.* **364**, 772–774 (2011).
19. Bacart, J., Corbel, C., Jockers, R., Bach, S. & Couturier, C. The BRET technology and its application to screening assays. *Biotechnol. J.* **3**, 311–324 (2008).
20. Breton, B. *et al.* Multiplexing of multicolor bioluminescence resonance energy transfer. *Biophys. J.* **99**, 4037–4046 (2010).
21. Kocan, M., See, H.B., Seeber, R.M., Eidne, K.A. & Pfleger, K.D. Demonstration of improvements to the bioluminescence resonance energy transfer (BRET) technology for the monitoring of G protein–coupled receptors in live cells. *J. Biomol. Screen.* **13**, 888–898 (2008).
22. James, J.R., Oliveira, M.I., Carmo, A.M., Iaboni, A. & Davis, S.J. A rigorous experimental framework for detecting protein oligomerization using bioluminescence resonance energy transfer. *Nat. Methods* **3**, 1001–1006 (2006).
23. Röring, M. *et al.* Distinct requirement for an intact dimer interface in wild-type, V600E and kinase-dead B-Raf signalling. *EMBO J.* **31**, 2629–2647 (2012).
24. Ritt, D.A., Monson, D.M., Specht, S.I. & Morrison, D.K. Impact of feedback phosphorylation and Raf heterodimerization on normal and mutant B-Raf signaling. *Mol. Cell Biol.* **30**, 806–819 (2010).
25. Dar, A.C. & Shokat, K.M. The evolution of protein kinase inhibitors from antagonists to agonists of cellular signaling. *Annu. Rev. Biochem.* **80**, 769–795 (2011).
26. Whittaker, S. *et al.* Gatekeeper mutations mediate resistance to BRAF-targeted therapies. *Sci. Transl. Med.* **2**, 35ra41 (2010).
27. Zhang, J.H., Chung, T.D. & Oldenburg, K.R. A simple statistical parameter for use in evaluation and validation of high throughput screening assays. *J. Biomol. Screen.* **4**, 67–73 (1999).
28. Tsai, J. *et al.* Discovery of a selective inhibitor of oncogenic B-Raf kinase with potent antimelanoma activity. *Proc. Natl. Acad. Sci. USA* **105**, 3041–3046 (2008).
29. Wan, P.T. *et al.* Mechanism of activation of the RAF-ERK signaling pathway by oncogenic mutations of B-RAF. *Cell* **116**, 855–867 (2004).
30. Lee, J.C. *et al.* A protein kinase involved in the regulation of inflammatory cytokine biosynthesis. *Nature* **372**, 739–746 (1994).
31. Hall-Jackson, C.A., Goedert, M., Hedge, P. & Cohen, P. Effect of SB 203580 on the activity of c-Raf *in vitro* and *in vivo*. *Oncogene* **18**, 2047–2054 (1999).
32. Kalmes, A., Deou, J., Clowes, A.W. & Daum, G. Raf-1 is activated by the p38 mitogen-activated protein kinase inhibitor, SB203580. *FEBS Lett.* **444**, 71–74 (1999).
33. McKay, M.M., Ritt, D.A. & Morrison, D.K. RAF Inhibitor-Induced KSR1/B-RAF binding and its effects on ERK cascade signaling. *Curr. Biol.* **21**, 563–568 (2011).
34. King, A.J. *et al.* Demonstration of a genetic therapeutic index for tumors expressing oncogenic BRAF by the kinase inhibitor SB-590885. *Cancer Res.* **66**, 11100–11105 (2006).
35. Wang, Z. *et al.* Structural basis of inhibitor selectivity in MAP kinases. *Structure* **6**, 1117–1128 (1998).
36. Anastassiadis, T., Deacon, S.W., Devarajan, K., Ma, H. & Peterson, J.R. Comprehensive assay of kinase catalytic activity reveals features of kinase inhibitor selectivity. *Nat. Biotechnol.* **29**, 1039–1045 (2011).
37. Packer, L.M. *et al.* Nilotinib and MEK inhibitors induce synthetic lethality through paradoxical activation of RAF in drug-resistant chronic myeloid leukemia. *Cancer Cell* **20**, 715–727 (2011).
38. Barrios-Rodiles, M. *et al.* High-throughput mapping of a dynamic signaling network in mammalian cells. *Science* **307**, 1621–1625 (2005).
39. Jeffrey, P.D. *et al.* Mechanism of CDK activation revealed by the structure of a cyclinA–CDK2 complex. *Nature* **376**, 313–320 (1995).
40. Sicheri, F. & Kuriyan, J. Structures of Src-family tyrosine kinases. *Curr. Opin. Struct. Biol.* **7**, 777–785 (1997).
41. Kornev, A.P., Haste, N.M., Taylor, S.S. & Eyck, L.F. Surface comparison of active and inactive protein kinases identifies a conserved activation mechanism. *Proc. Natl. Acad. Sci. USA* **103**, 17783–17788 (2006).
42. Kornev, A.P. & Taylor, S.S. Defining the conserved internal architecture of a protein kinase. *Biochim. Biophys. Acta* **1804**, 440–444 (2010).
43. Bukhtiyarova, M., Karpusas, M., Northrop, K., Namboodiri, H.V. & Springman, E.B. Mutagenesis of p38α MAP kinase establishes key roles of Phe169 in function and structural dynamics and reveals a novel DFG-OUT state. *Biochemistry* **46**, 5687–5696 (2007).
44. Axten, J.M. *et al.* Discovery of 7-methyl-5-(1-{[3-(trifluoromethyl)phenyl] acetyl}-2,3-dihydro-1H-indol-5-yl)-7H-p yrrolo[2,3-d]pyrimidin-4-amine (GSK2606414), a potent and selective first-in-class inhibitor of protein kinase r (PKR)-like endoplasmic reticulum kinase (PERK). *J. Med. Chem.* **55**, 7193–7207 (2012).
45. Dey, M. *et al.* Mechanistic link between PKR dimerization, autophosphorylation, and eIF2α substrate recognition. *Cell* **122**, 901–913 (2005).
46. Taylor, S.S., Haste, N.M. & Ghosh, G. PKR and eIF2α: integration of kinase dimerization, activation, and substrate docking. *Cell* **122**, 823–825 (2005).
47. Korennykh, A.V. *et al.* The unfolded protein response signals through high-order assembly of Ire1. *Nature* **457**, 687–693 (2009).
48. Sen, B. *et al.* Kinase-impaired BRAF mutations in lung cancer confer sensitivity to dasatinib. *Sci. Transl. Med.* **4**, 136ra170 (2012).
49. Dar, A.C., Dever, T.E. & Sicheri, F. Higher-order substrate recognition of eIF2α by the RNA-dependent protein kinase PKR. *Cell* **122**, 887–900 (2005).

Acknowledgments

We thank B. Breton and M. Audet for advice with the BRET2 system, D. Uehling and co-workers at the Ontario Institute for Cancer Research for GSK2606414, and the Institut de recherche en immunologie et en cancérologie (IRIC) high-throughput screening platform. IRIC is supported by the Canadian Center of Excellence in Commercialization and Research, the Canada Foundation for Innovation and by the Fonds de Recherche du Québec en Santé. H.L. is a recipient of Cancer Research Society and Canadian Institutes for Health Research (CIHR) Banting postdoctoral fellowships. N.T. is a recipient of the CIHR Canadian Graduate Scholarship. M.B., F.S. and M.T. hold Canada Research Chairs. This work was supported by operating funds from the Canadian Cancer Society to M.T. (018046) and from the CIHR to M.T. (MOP119443) and F.S. (MOP36399).

Author contributions

H.L., N.T., F.S. and M.T. designed the experiments and wrote the manuscript. M.B. contributed to the theoretical framework surrounding BRET assay development and participated in the analysis of the BRET data and in the revision of the manuscript. H.L., with assistance from G.G., A.P., S.G. and J.D., conducted cell-based BRET analyses, the high-throughput chemical screen and TR-FRET *in vitro* binding assays. N.T., with assistance from D.Y.L.M., J.J.L. and H.L., performed AUC and X-ray structure analyses.

Competing financial interests

The authors declare competing financial interests: details accompany the online version of the paper.

Additional information

Supplementary information is available in the online version of the paper. Reprints and permissions information is available online at http://www.nature.com/reprints/index.html. Correspondence and requests for materials should be addressed to M.T.

ONLINE METHODS

Plasmids. All of the constructs were introduced in pCDNA3.1-based vectors (Invitrogen). The CAAX box of human KRAS (last 20 amino acids) was added to ARAF$^{301–606}$, BRAF$^{448–766}$, CRAF$^{340–648}$, KSR1$^{602–921}$ or KSR2$^{657–950}$ kinase domains by PCR, and BRET fusions were generated by inserting these kinase domains or full-length BRAF and CRAF proteins between KpnI and XbaI in a pCDNA3.1-Hygro plasmid already containing a N- or C-terminal cassette containing either the GFP10 or *Renilla* luciferase II cDNA[20] (oligonucleotides used are listed in **Supplementary Table 6**). Flag-tagged BRAF was generated by PCR and cloned in the same plasmid backbone between KpnI and XbaI sites. KRAS, HRAS and NRAS mCherry fusions were also cloned between KpnI and XbaI and were site-directed mutagenized by PCR using standard procedures. BRAF$^{444–723}$, used in AUC analysis and crystallography, was cloned with 16 solubilization mutations[28] (I543A, I544S, I551K, Q562R, L588N, K630S, F667E, Y673S, A688R, L706S, Q709R, S713E, L716E, S720E, P722S and K723G), referred to as BRAF$_{16mut}$, into pPROEX-HTa (Invitrogen) between NcoI and NotI sites. Mouse PERK$^{577–1082}$, with flexible loop residues 661–875 removed (here after referred to as PERK), was cloned into a SUMO-cleavable GST fusion vector.

Cell culture, transfection and preparation for BRET assays. HEK293T and COLO-205 cells were maintained in DMEM supplemented with 10% FBS and penicillin-streptomycin. HCT-116 cells were cultured in McCoy's medium with 10% FBS and penicillin-streptomycin. For titration curves, 3×10^5 cells were seeded in six-well plates and transfected the next day with polyethylenimine (PEI)[50] at 1 µg/µl (see **Supplementary Note 1**). For dose-response curves, 2.5×10^6 cells were seeded in 100-mm plates and transfected with a total of 4 µg of DNA. Forty-eight hours after transfection, cells were washed, resuspended in Tyrode's buffer (10 mM HEPES, 137 mM NaCl, 2.68 mM KCl, 0.42 mM NaH_2PO_4, 1.7 mM $MgCl_2$, 11.9 mM $NaHCO_3$ and 5 mM glucose), counted and transferred to white opaque microtiter plates (BD Biosciences). A similar procedure was conducted for the high-throughput chemical screening, except that cells were cultured in CellStacks (Corning) (**Supplementary Note 1**).

BRET measurements. BRET signals and luciferase activity were read 15 min after addition of 2.5 µM Coelenterazine 400a (Biotium) using a Mithras LB940 plate reader (Berthold Technologies) equipped with BRET1 emission filter set (donor: 480nm ± 20 nm; acceptor: 530 nm ± 20 nm). BRET signals emitted by RlucII-GFP10 pairs (BRET2 probes) can be read with either BRET1 or BRET2 filter sets[20]. The main difference is that the calculated BRET ratio is higher with BRET1 filters than with BRET2 filters (donor: 400 nm ± 20 nm; acceptor: 510 nm ± 20 nm) because only the shoulder of the RlucII emission spectrum is captured, whereas the full peak of RlucII would be detected with a 400-nm filter. In addition, the BRET1 filter set produced slightly better *Z* factors. BRET signals correspond to the light emitted by the GFP10 acceptor constructs (530 nm ± 20 nm) upon addition of Coelenterazine 400a divided by the light emitted by the RlucII donor constructs (480 nm ± 20 nm). Specific BRET signals referred to as BRET in the text and figures correspond to total BRET signals measured from donor- or acceptor-transfected samples minus background BRET signals measured from samples transfected with donor (RlucII constructs) alone. Total GFP10 or mCherry was detected on a FlexStation II (Molecular Devices) with excitation and emission peaks set at 400 nm and 510 nm and at 580 nm and 635 nm, respectively. Total intrinsic GFP10 (expressed as relative fluorescence unit; RFU) and RlucII (relative luminescence unit; RLU) signals were used as a proxy to ensure that similar protein expression between comparable probes were used in titration experiments. In titration experiments whereby GFP10 acceptor constructs are titrated in, BRET signals (*y* axis) were plotted in relation to the increasing ratio of total GFP10 signal (RFU)/total luciferase signal (RLU) (*x* axis: [acceptor]/[donor]). BRET-based dose-response experiments were expressed as BRET fold increase and were calculated by dividing the BRET of compound-treated cells by the BRET of control DMSO-treated cells. Finally, for high-throughput chemical screening (**Supplementary Table 7**), BRET measurements were acquired using a SpectramaxL luminometer (Molecular Devices), and GFP10 signals were read on an EnVision (Perkin Elmer) plate reader. Data for the chemical screen were expressed as percent of BRET induction and were calculated as follows: $(100 \times (BRET_{COMPOUND} / BRET_{DMSO})) - 100$; where $BRET_{COMPOUND}$ corresponds to the BRET signals obtained for the compound-treated cells, and $BRET_{DMSO}$ corresponds to the BRET signals obtained for control DMSO-treated cells. Detailed BRET procedures are described in **Supplementary Note 1**.

Co-immunoprecipitation, western blotting and AlphaScreen assays. Co-immunoprecipitation and western blotting procedures were essentially conducted as follows. To prepare cell lysates, cells were washed once in cold 1× phosphate-buffered saline (PBS) and then directly lysed on plates by adding 1 ml of Igepal lysis buffer (20 mM Tris at pH 8.0, 137 mM NaCl,10% glycerol, 1% Igepal CA-630, 2 mM EDTA, 1× phosphatase inhibitor cocktail (Sigma), 1 mM sodium vanadate, 20 µM leupeptin, aprotinin (0.15 U/ml) and 1 mM phenylmethylsulfonyl fluoride (PMSF)). Lysing cells were incubated for 10 min at 4 °C with gentle rocking, collected and spun at 14,000*g*, 4 °C for 10 min. For co-immunoprecipitations, primary antibodies were added to fresh cell lysates and incubated at 4 °C for 1 h. Protein A/G agarose beads (Santa Cruz Biotechnology) were then added, and gently rocked at 4 °C for an additional 3 h. Immunoprecipitates were washed three times with cold lysis buffer. Flag-tagged complexes were eluted with 3× Flag peptide (Sigma) before gel electrophoresis. Cell lysates or immunoprecipitated proteins were resolved on 8% SDS-PAGE, transferred to nitrocellulose membranes (Dupont) and probed using appropriate primary antibodies. All of the antibodies were diluted in Tris-buffered saline (TBS) supplemented with 0.2% Tween. *Renilla* luciferase–specific (anti-Renilla) 5B11.2 (Millipore), anti-GFP clones 7.1/13.1 (Roche), anti-phosphoERK1/2 (Sigma), anti-phosphoMEK (Cell Signaling Technology) and anti-MEK1 (610121; BD Biosciences) were used at a dilution of 1:2,000. Anti-Flag M2 (Sigma) was used at a 1:5,000 dilution. Secondary anti-mouse and anti–rabbit-HRP (Santa Cruz Biotechnology) were used at a 1:10,000 dilution in TBS-0.2%Tween. Phospho-ERK analysis was conducted on 40,000 cells cultured overnight in 96-well plates and treated with the indicated compound concentrations for 2 h. Phospho-ERK1/2 AlphaScreen (PerkinElmer) assays were performed according to the manufacturer's specifications.

Inhibitors used in this study. PLX4720, GDC-0879 and AZ-628 were obtained from Axon Medchem. Sorafenib, imatinib, dasatinib, nilotinib, pazopanib and tivozanib were purchased from LC laboratories. SB202190 and SB203580, BIRB796, SB590885 were from Selleck Chemicals. TWS119, MNK1 inhibitor and VEGFR inhibitor II were from Calbiochem. All compounds were at least 95% pure as evaluated by HPLC (**Supplementary Table 8**). For dose-response experiments, serial dilutions of all of the drugs were prepared in DMSO, and 1:100 dilutions were prepared in Tyrode's buffer before addition to 90 µl of cell suspensions in Tyrode's buffer (1×10^6 cells/ml) at a 1:10 dilution for 2 h. GGTI-298 and FTI-277 (Sigma-Aldrich) were also prepared in DMSO. The compound library used for high-throughput screening was provided by the IRIC HTS facility and was obtained from various sources (http://www.iric.ca/en/research/core-facilities/high-throughput-screening/?section=technologies/). The focused kinase inhibitor library was assembled from the EMD chemicals InhibitorSelect library, and various other inhibitors were obtained from LC laboratories (**Supplementary Data Set 1** and **Supplementary Table 7**). The GSK2606414 analog referred to as compound 39 (5-(1-{[3-fluoro-5-(trifluoromethyl)phenyl]acetyl}-2,3-dihydro-1H-indol-5-yl)-7-methyl-7H-pyrrolo[2,3-d]pyrimidin-4-amine) was kindly provided by D. Uehling (Ontario Institute for Cancer Research, Toronto).

Protein purification. TEV-cleavable His_6-tagged BRAF$_{16mut}$ was expressed in BL21(DE3)-RIL bacterial expression cells, purified with nickel affinity chromatography, TEV-cleaved overnight and purified through gel filtration chromatography into a final buffer of 15 mM HEPES, pH 7.5, 200 mM NaCl, 10 mM DTT and 5% glycerol. SUMO protease–cleavable GST tagged PERK was expressed in BL21(DE3)-RIL cells, purified by glutathione affinity chromatography, treated with SUMO protease overnight and purified through gel filtration chromatography into a final buffer of 100 mM HEPES pH 7, 100 mM NaCl and 1 mM TCEP. Following gel filtration, protein fractions corresponding to >95% purity were pooled and concentrated to 20 mg/mL, and then flash frozen in liquid nitrogen.

Protein crystallization and structural analysis. BRAF$_{16mut}$ (156 µM, 5 mg/mL) was co-crystallized with 230 µM BIRB796 at 4°C in 0.1M BisTris propane, pH 8, and 30% PEG 3350 using the hanging drop method. X-ray diffraction data were collected on a flash-frozen crystal cryo-protected in mother liquor containing 22% glycerol at the Advanced Photon Source (NECAT beamline 24-ID). Data reduction was performed using HKL2000 (HKL Research Inc.). The BRAF$_{16mut}$-BIRB796 co-structure was solved by molecular replacement using the structure in PDB 3C4C as a search model in Phaser[51]. Model refinement was performed using Phenix 1.7.1 (ref. 51).

Analytical ultracentrifugation. Sedimentation velocity analytical ultracentrifugation was performed with a Beckman ProteomeLab XL-I at 42,000 r.p.m. Data were obtained after 7.5 h of centrifugation at 20 °C by monitoring the relative refractive index between sample and blank. Various concentrations of $BRAF_{16mut,}$ ranging from 0.78 μM to 25 μM, were tested minimally in duplicate in AUC buffer ($BRAF_{16mut}$: 15 mM HEPES. pH 7, 200 mM NaCl, 3 mM DTT; PERK: 20 mM HEPES, pH 7.5, 150 mM NaCl, 1 mM TCEP) in the presence or absence of 40 μM inhibitor compound, or 200 μM AMP-PNP with 200 μM $MgCl_2$, or 200 μM ADP with 200 μM $MgCl_2$. AUC analyses of PERK used identical conditions as per $BRAF_{16mut}$ with the exception that ADP analyses were performed with 500 μM ADP with 2 mM $MgCl_2$. The AUC experimental conditions for $BRAF_{16mut,}$ were extensively optimized to maximize protein stability for the duration of the AUC analysis and differed from those used previously for a shorter BRAF construct[7] in temperature (4°C), duration of centrifugation (14 d per sedimentation equilibrium analysis) and buffer composition (20 mM Tris, pH 7.0, 200 mM NaCl, 5% glycerol and 1.5 mM TCEP).

Drug-binding assay by TR-FRET. For drug-binding assays, a procedure similar to the LanthaScreen Eu Kinase Binding Assay for BRAF (Invitrogen) was used. Purified His_6-tagged $BRAF^{444–723}$ kinase domain (50 nM final concentration) was co-incubated with 2 nM LANCE Europium-coupled anti-His (PerkinElmer; AD0205), 60 nM Alexa Fluor 647–labeled kinase tracer 178 (Invitrogen; PV5593) and varying concentrations of kinase inhibitors for 1 h at room temperature in kinase buffer (50 mM HEPES, pH 7.5, 100 mM NaCl, 3mM DTT, 10 mM $MgCl_2$, 1mM EDTA and 0.01% Brij-35). Each experiment included control wells (triplicates) containing the LANCE antibody and Alexa Fluor 647–labeled kinase tracer 178 alone; the average signal of the blank wells was subtracted from each data point. TR-FRET was read on an EnVision (PerkinElmer) plate reader with a 340 ± 30 nm excitation filter. The emission of Alexa Fluor 647 signal was monitored with a 665 ± 10 nm filter, and the Europium emission signal was acquired using a 615 ± 10 nm filter. The TR-FRET signal was calculated by dividing the emission signal at 665 nm by the emission at 615 nm. The relative reduction in TR-FRET signal was calculated by normalizing each data point to the corresponding point in the DMSO vehicle–treated wells.

Data analysis and structure rendering. BRET titration curves allow extrapolation of two key parameters, namely $BRET_{50}$ and $BRET_{max}$, which can be used to assess pharmacological or genetic alterations of interacting proteins. The $BRET_{50}$ corresponds to the ratio of acceptor construct over donor construct required to attain 50% of the maximum BRET signal. It is essentially dictated by the relative affinity of interacting BRET pairs and their propensity to localize together. In contrast, the $BRET_{max}$ represents the maximum BRET signal strength obtained with saturating amounts of the acceptor probe. This parameter depends on the distance between BRET pairs, their relative orientation and the proportion of donor proteins engaged in dimerization[19,52].

Raw data were analyzed using the Prism 5.04 software (GraphPad Software). $BRET_{max}$, $BRET_{50}$ parameters were derived from a one-site binding hyperbolic fitting of the data, and EC_{50} values were calculated using a log(agonist) versus response fitting. Significance in $BRET_{50}$ and $BRET_{max}$ differences between BRAF mutants and after drug treatments was assessed using an F-test. Heat map displays were generated using the Treeview program (http://www.eisenlab.org/eisen/?page_id=42). All of the protein structure representations were prepared using PyMol (Schrödinger). AUC data were processed using SEDFIT (National Institute of Health) to calculate a continuous c(s) distribution. Solute partial specific volume, buffer density and buffer viscosity were calculated using Sednterp (Thomas Laue).

50. Boussif, O. *et al.* A versatile vector for gene and oligonucleotide transfer into cells in culture and *in vivo*: polyethylenimine. *Proc. Natl. Acad. Sci. USA* **92**, 7297–7301 (1995).
51. Adams, P.D. *et al.* PHENIX: a comprehensive Python-based system for macromolecular structure solution. *Acta Crystallogr. D Biol. Crystallogr.* **66**, 213–221 (2010).
52. Ciruela, F. Fluorescence-based methods in the study of protein-protein interactions in living cells. *Curr. Opin. Biotechnol.* **19**, 338–343 (2008).

doi:10.1038/nchembio.1257